Driven transport on parallel lanes with particle exclusion and obstruction

Anna Melbinger,[1] Tobias Reichenbach,[2] Thomas Franosch,[1,3] and Erwin Frey[1]

[1]*Arnold Sommerfeld Center for Theoretical Physics (ASC) and Center for NanoScience (CeNS), Department of Physics,
Ludwig-Maximilians-Universität München, Theresienstraße 37, D-80333 München, Germany*
[2]*Laboratory of Sensory Neuroscience, The Rockefeller University, 1230 York Avenue, New York, New York 10065, USA*
[3]*Institut für Theoretische Physik, Friedrich-Alexander-Universität Erlangen-Nürnberg, Staudtstraße 7, D-91058 Erlangen, Germany*

We investigate a driven two-channel system where particles on different lanes mutually obstruct each other's motion, extending an earlier model by Popkov and Peschel [Phys. Rev. E **64**, 026126 (2001)]. This obstruction may occur in biological contexts due to steric hindrance where motor proteins carry cargos by "walking" on microtubules. Similarly, the model serves as a description for classical spin transport where charged particles with internal states move unidirectionally on a lattice. Three regimes of qualitatively different behavior are identified, depending on the strength of coupling between the lanes. For small and large coupling strengths the model can be mapped to a one-channel problem, whereas a rich phase behavior emerges for intermediate ones. We derive an approximate but quantitatively accurate theoretical description in terms of a one-site cluster approximation, and obtain insight into the phase behavior through the current-density relations combined with an extremal-current principle. Our results are confirmed by stochastic simulations.

I. INTRODUCTION

Driven diffusive systems are of importance in various fields of physics and biology [1,2], since they serve as simplistic models for biological transport phenomena [3–6], traffic flow [7–10], fast ionic conductors [11], as well as quasiclassical spin transport [12]. Furthermore, they provide valuable insights into nonequilibrium statistical mechanics. As an example, and in contrast to equilibrium systems, their bulk behavior is sensitive to the boundaries [13]. Boundary induced phase transitions in one dimension may emerge resulting in complex phase behavior.

The most prominent example of driven lattice gases, the totally asymmetric exclusion process (TASEP), was originally proposed as a simple model for the motion of multiple ribosomes along a mRNA strand during protein translation [14]. In this model, particles move unidirectionally along a one-dimensional lattice, provided the next site is empty. Exact solutions, e.g., by employing the Bethe ansatz [15] or a matrix product ansatz [16], are feasible, yet much insight can readily be obtained from simple mean-field considerations [2].

Intracellular transport constitutes another fascinating biological application [17] of driven systems. Here, molecular motors such as kinesin or dynein, driven by the hydrolysis of adenosine triphosphate (ATP), move unidirectionally along microtubules [3]. Macromolecules or other cellular constituents, which often are too large to diffuse fast enough through the crowded cytosol, are carried by motor proteins, and are then actively transported to the location where they are needed. Recent theoretical studies motivated by these processes have investigated the influence of attachment and detachment of the motors to the microtubules [18–22], extended particles [23], the influence of defects on the track [24–26], and the competition between different motor species [27,28]. Further attention has been paid to transport along several coupled channels where particles move in parallel. This coupling can be either achieved by allowing lane-switching events [12,29–37] or by a possible influence of a particle in

one channel on the motion in the other channel [7,38]. Here we consider the latter case and investigate how mutual obstruction of motor proteins on neighboring lanes, for example, stemming from large cargos attached to them, affects the transport properties of the system.

Driven diffusive systems may also serve as a description for spin transport with possible applications in the field of spintronics. For instance, such spin currents flow in a chain of quantum dots where electrons are driven by an external voltage in a way that only the lowest energy levels can be occupied [39]. Hence not more than one electron of each internal state is permitted per site and electrons located in the immediate vicinity repel each other due to Coulomb interaction. A model taking Pauli's exclusion principle into account while ignoring phase coherence has been investigated recently [12,30,31], yet Coulomb blockade has been neglected. In the present paper we focus on the influence of a mutual obstruction mimicking, for example, Coulomb interaction. To identify its effect on the collective transport properties in the clearest way, we disregard spin-flip events which can cause intriguing behavior on their own [12,30,31].

A simple lattice model that incorporates mutual obstruction on two lanes has been investigated by Popkov and Peschel [7]. The steric hindrance there is manifested in the hopping rates that explicitly depend on the configuration on the opposing lane. As a consequence of this coupling of the lanes, a variety of peculiar phases arises which has been neatly rationalized in terms of a cluster approximation. Particularly, symmetry breaking, which arises even though the boundary conditions are symmetric, is observed and analyzed.

In this paper we extend the model of Ref. [7] by considering asymmetric boundary conditions and rates instead of reservoirs at the right boundary. We introduce the model in Sec. II, both in the two-lane and in the spin-transport picture. In Sec. III we describe the stochastic simulations and provide first insights in how particle obstruction affects the behavior. Namely, we identify three regimes of qualitatively different behavior. In

Sec. IV, we analytically compute the current-density relations within a one-site cluster approximation. Section V presents a discussion on how the current-density relation, obtained via an extremal-current principle, allows us to identify the system's different phases and to analytically predict the phase diagram. We summarize our main findings in Sec. VI and provide a brief conclusion.

II. MODEL

We examine a driven diffusive system which serves as a minimal model for the transport on two parallel lanes, which are coupled by a repulsive short-range interaction. The same model describes classical driven spin transport with Coulomb blockade. In the following we specify the dynamics in detail, presenting both the two-lane and the spin-transport representation.

A. Two-channel representation

Consider particle transport along two parallel channels, each of them containing N discrete lattice sites; see Fig. 1. Each site may contain at most one particle (on-site exclusion), such that the occupation number of site i on the upper (lower) channel, $n_i^\uparrow (n_i^\downarrow)$, can only take values 0 or 1, corresponding to a vacant or an occupied site, respectively.

Particles enter from two entangled reservoirs located at the left-hand side of the system. At each time step, the reservoir is in one of the four possible states: (i) double occupation with probability κ^*, (ii) only the upper reservoir is occupied with probability $\rho_{\text{res}}^\uparrow - \kappa^*$, (iii) only the lower reservoir is occupied with probability $\rho_{\text{res}}^\downarrow - \kappa^*$, and (iv) both reservoir sites are empty with probability $1 - \rho_{\text{res}}^\uparrow - \rho_{\text{res}}^\downarrow + \kappa^*$. Thus $\rho_{\text{res}}^\uparrow$ and $\rho_{\text{res}}^\downarrow$ are the average densities on the upper and lower reservoir, respectively, and κ^* corresponds to the double-occupation density in the reservoir.

In bulk, particles move unidirectionally to the right. Due to obstruction, the hopping rate thereby depends on the particle configuration at the other lane. A particle attempting to proceed by one site is obstructed if a particle resides on the subsequent site of the other channel. However, this obstruction is relevant only when the particle does not experience obstruction in its current position, meaning when its current neighboring site on
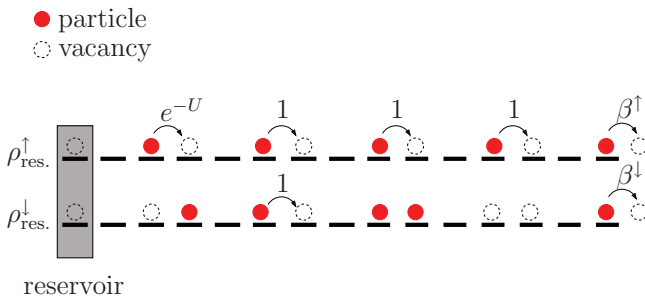

FIG. 1. (Color online) Illustration of the two-lane representation. Particles enter from two reservoirs at the left boundary with densities $\rho_{\text{res}}^\uparrow, \rho_{\text{res}}^\downarrow$. In bulk, hopping rates depend on the particle configuration of the, respective, other lane. At the right boundary particles leave at rates $\beta^\uparrow, \beta^\downarrow$.
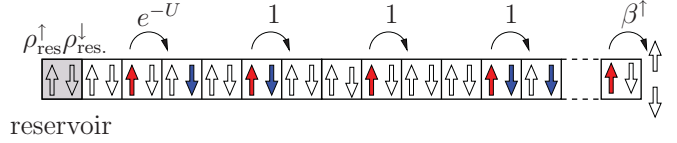

FIG. 2. (Color online) Illustration of an exclusion model with two internal states, adopting the language of spin transport. Particles in state $\uparrow (\downarrow)$ enter the system at the left boundary from a reservoir with density $\rho_{\text{res}}^\uparrow (\rho_{\text{res}}^\downarrow)$ and leave at the right boundary with rate $\beta^\uparrow (\beta^\downarrow)$. In bulk, particles hop to the right, always respecting Pauli's exclusion principle. If an unpaired particle moves to a site which is already occupied by a particle of the other spin state the hopping rate is decreased to e^{-U}; otherwise, the hopping rate is set to 1.

the other channel is empty. We model this effect by reducing the hopping rate to a value e^{-U} $(U > 0)$ in this case, while the rate is unity for all other configurations. In the biological context of molecular motors walking along microtubuli, the reduced hopping rate corresponds to the spatial obstruction stemming from large cargos attached to motor proteins.

Last, the rules of the model are completed by specifying how particles leave the system after traversing the bulk. Here, we consider that particles at the right boundary leave with the exiting rates $\beta^\uparrow, \beta^\downarrow$ in contrast to [7] (see Fig. 1).

B. Spin-transport representation

The model can be readily interpreted in the context of spin transport where it serves as a description for classical spin currents (see Fig. 2). The analogy to the two-channel picture is the following: A particle situated at the upper (lower) lane maps to a particle with spin up (spin down). At the left boundary particles enter from a spin reservoir with densities $\rho_{\text{res}}^\uparrow, \rho_{\text{res}}^\downarrow$. Having traversed the lattice, they leave the system at the right boundary with exiting rates $\beta^\uparrow, \beta^\downarrow$. In bulk, the particles move to the right always respecting Pauli's exclusion principle, i.e., only one particle per internal state is permitted per site. According to the two-lane representation, the hopping rates depend on the particle configuration of the system. A short-range repulsive interaction reduces the hopping rate for an unpaired particle onto a site which is already occupied by a particle of the other spin state to e^{-U}, as compared to 1 for the other configurations. The parameter $U > 0$ may be viewed as an effective interaction potential, originating from a repulsive Coulomb interaction, where particles on the same site (though different spin states) gain potential energy. In this context, one can also consider an increased hopping rate away from a double occupation, yet, one can show that this does not change our results qualitatively [40]. For clarity, we employ only the two-channel representation in the following.

A model similar to the one introduced above was recently proposed in [7]. However, only symmetric situations were considered with entrance/exit reservoirs that were equal an both lanes. As a further difference to our model the authors did model the exiting processes through reservoirs at the right side instead of exiting rates. Because we explicitly investigate the asymmetric case, with entrance and exit properties that differ for the two lanes, and because of our usage of exit rates we find a multitude of interesting phenomena, summarized in Sec. VI. The asymmetry between the two lanes requires

a two-dimensional generalization of the extremal-current principle. The derivation of this two-dimensional extremal-current principle constitutes a key result of our work; we show how it successfully describes much of the system's behavior.

III. CLASSIFICATION OF THE SYSTEM'S SENSITIVITY ON THE POTENTIAL

The steady-state bulk densities $\rho_i^\uparrow = \langle n_i^\uparrow \rangle, \rho_i^\downarrow = \langle n_i^\downarrow \rangle$, where $\langle \cdot \rangle$ indicates a coarse-grained time average, constitute key observables. Because of particle conservation, their temporal evolution can be obtained from the particle flux j_{i-1} onto site i and the one away from it, j_i:

$$
\begin{aligned}
\partial_t \rho_i^\uparrow &= j_{i-1}^\uparrow - j_i^\uparrow, \\
\partial_t \rho_i^\downarrow &= j_{i-1}^\downarrow - j_i^\downarrow.
\end{aligned}
\tag{1}
$$

The currents, $j_i^\uparrow, j_i^\downarrow$, contain correlations between neighboring sites on the lattice. To find an analytic description, these correlations have to be accounted for by a suitable closure relation, e.g., by a mean-field approximation or a one-site cluster approximation.

Stochastic simulations provide another route to gain insight into the system's behavior. In this section we first detail the simulation algorithm, and then describe three classes of behavior that emerge for different interaction strength.

A. Stochastic simulations

We have determined the system's stationary state via stochastic simulations with random sequential updating, using the dynamic rules introduced in the previous section and employing the Gillespie algorithm [41,42]. We have performed time averages over about 10^5 time intervals, each containing $10 \times L$ time steps and the lattice size is set to $L = 1000$. At the left boundary, the reservoir dynamics is specified in terms of the three parameters, $\rho_{\text{res}}^\uparrow, \rho_{\text{res}}^\downarrow$, and κ^*. Here, we restrict the discussions to the case of *relaxed* reservoirs, where the correlations in the reservoirs reflect the ones in bulk, which is particularly illuminating and amenable to a theoretical description. Then, the double occupation density can be determined from the average densities, $\rho_{\text{res}}^\uparrow, \rho_{\text{res}}^\downarrow$ according to Eq. (A4) derived in the Appendix. In general, and apart from boundary effects such as boundary layers, we found constant density profiles in the system. To determine the corresponding value of the average density in bulk for constant density profiles, we only considered the $0.2 \times L$ sites in the center of both channels. Our simulations confirm to a large extent the analytic approximations which are to be discussed in the following sections.

B. Dependence on the interaction strength U

In the case of vanishing coupling, i.e., $U = 0$, the system simply corresponds to two uncoupled TASEPs. In the presence of obstruction, and thereby coupling between both channels, this picture changes drastically upon increasing the effective interaction strength. Our stochastic simulations show three regimes of qualitatively different behavior, which are illus-
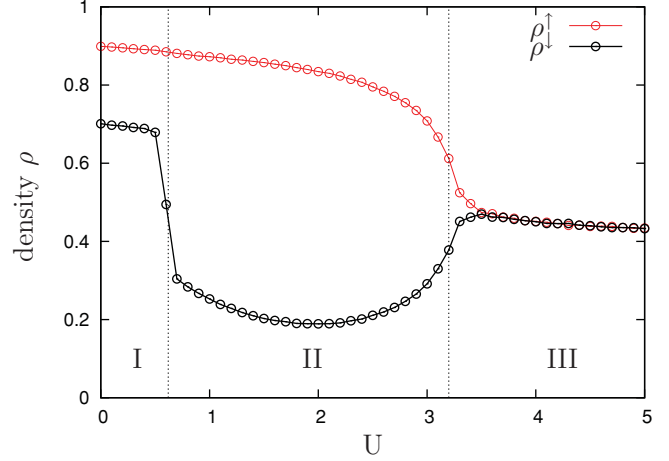

FIG. 3. (Color online) Average bulk densities obtained by stochastic simulations on the upper (red, gray) and lower lane (black) for varying potential strength U. The parameters are $\rho_{\text{res}}^\uparrow = \rho_{\text{res}}^\downarrow = 0.5$, $\beta^\uparrow = 0.1$, and $\beta^\downarrow = 0.3$. Three regimes of qualitatively different behavior emerge. In the first one (I) the system qualitatively behaves like two uncoupled systems. In regime II, the density in the lower channel strongly decreases, while the density in the upper channel is still large. This nontrivial behavior is discussed in detail in Secs. IV and V. In regime III, for strong coupling, the system behaves like a one-channel TASEP.

trated in Fig. 3. In the following, we discuss these regimes, and provide a mapping on TASEP for two of them.

1. Weak coupling

In the first regime (I), for small coupling strength U, the system almost behaves like two uncoupled lanes, except for the fact that the densities are slightly reduced. This regime can be well described by a simple mean-field approximation, where correlations between different lattice sites, $i \neq j$, are neglected, $\langle n_i^{\uparrow(\downarrow)} n_j^{\uparrow(\downarrow)} \rangle \approx \langle n_i^{\uparrow(\downarrow)} \rangle \langle n_j^{\uparrow(\downarrow)} \rangle$, or by a one-site cluster approximation which is to be discussed in detail in the following section. In this regime the phase behavior qualitatively corresponds to the one already known from TASEP. On a quantitative level, differences arise as the phase transition lines are shifted compared to the uncoupled case.

2. Intermediate coupling

In regime II, the one of intermediate coupling strength, an intriguing phase behavior emerges. For instance, for the set of parameters shown in Fig. 3 , the density in the upper channel remains rather undisturbed by the obstruction, while the one in the lower channel drops to a comparatively small value. The nontrivial behavior in regime II is caused by the influence of the potential on the transport properties in bulk as well as on the boundaries. Especially, the exiting current is strongly influenced by the interaction potential resulting in smaller densities at the right boundary than expected for uncoupled systems. We rationalize this behavior in the following section. Because the system operates far from equilibrium, this change in the boundary conditions has a strong impact on the system.

Second, the transport properties in bulk also react sensitively to the coupling. As discussed in detail in the following

section, this causes changes in the currents' dependences on the bulk densities for potentials larger than a critical strength $U_C = \ln 4 \approx 1.4$.

Furthermore, other intriguing phenomena, such as domain walls between a low and a high density phase, are found. Also, there exist phases where the system depends sensitively on both boundaries, namely, the total current of the system is fixed by the right boundary while the exact value of the densities in bulk depends on the left boundary.

3. Strong coupling

A further increase in U leads to strong obstruction between the lanes with new qualitative behavior. In this regime of strong coupling (III) double occupancy of a site almost never occurs due to the vanishing hopping rate e^{-U} that would yield this configuration. Therefore the transport properties of two coupled channels is similar to a single-channel TASEP. This mapping cannot always be performed if the boundaries are reservoirs. It then only holds for the special case of small reservoir densities. Otherwise correlations between the upper and the lower reservoir are large. They are transported in the bulk and there destroy the effective one-lane behavior. Especially, the behavior shown in Fig. 3 would drastically change, if the exiting rates $\beta^\uparrow = 0.1$ and $\beta^\downarrow = 0.3$ would be replaced by the corresponding right reservoirs, namely the description holding for regime II would then apply and the bulk densities would not show the one-channel behavior.

Introducing the total density, $\tau_i = \langle n_i^\uparrow + n_i^\downarrow \rangle$, and performing the limit $e^{-U} \to 0$, which yields $\langle n_i^\uparrow n_i^\downarrow \rangle = 0$, in the expression for the currents [Eq. (A1)], one can identify the following mean-field current-density relation, already familiar from TASEP:

$$J = \tau(1 - \tau). \tag{2}$$

Due to the large potential in this regime, particles on different lanes are not able to "overtake" each other. Hence the ratio of the densities in both channels is fixed to the value given by the reservoir densities at the left boundary,

$$\frac{\rho^\uparrow}{\rho^\downarrow} = \frac{\rho_{\text{res}}^\uparrow}{\rho_{\text{res}}^\downarrow}. \tag{3}$$

In Fig. 3 we have used equal reservoir densities for the upper and the lower lane, and as a consequence the bulk densities of both lanes are equal.

The exact phase behavior can be determined by relating the boundary conditions of the two-lane system to the corresponding boundary conditions of the effective one-lane TASEP, for which the exact phase diagram is known. For reservoir densities $\rho_{\text{res}}^\uparrow, \rho_{\text{res}}^\downarrow < 0.5$, the effective entering rate is obtained by simply adding both reservoir densities:

$$\alpha_{\text{eff}} = \rho_{\text{res}}^\uparrow + \rho_{\text{res}}^\downarrow. \tag{4}$$

The effective exiting rate displays a more complex dependence on the boundary processes because the individual exiting rates influence the exiting current on both channels. To find a good estimate of the effective exiting rate, we consider the average time a particle spends on the last lattice site before it leaves the channel. This time is the inverse of the corresponding exiting rate. The weight of both waiting times is given by the

ratio of particles in the upper and lower lane. Hence a fraction $\rho_{\text{res}}^\uparrow / (\rho_{\text{res}}^\uparrow + \rho_{\text{res}}^\downarrow)$ of all particles spend $1/\beta^\uparrow$ time units on the last lattice site, and a fraction $\rho_{\text{res}}^\downarrow / (\rho_{\text{res}}^\uparrow + \rho_{\text{res}}^\downarrow)$ of the particles $1/\beta^\downarrow$ time units. The average time is the sum of both times weighted with their frequency,

$$\frac{\rho_{\text{res}}^\uparrow}{\rho_{\text{res}}^\uparrow + \rho_{\text{res}}^\downarrow} \frac{1}{\beta^\uparrow} + \frac{\rho_{\text{res}}^\downarrow}{\rho_{\text{res}}^\uparrow + \rho_{\text{res}}^\downarrow} \frac{1}{\beta^\downarrow},$$

yielding the effective exiting rate,

$$\beta_{\text{eff}} = \frac{(\rho_{\text{res}}^\uparrow + \rho_{\text{res}}^\downarrow)\beta^\uparrow \beta^\downarrow}{\rho_{\text{res}}^\uparrow \beta^\downarrow + \rho_{\text{res}}^\downarrow \beta^\uparrow}. \tag{5}$$

For reservoir densities $\rho_{\text{res}}^\uparrow, \rho_{\text{res}}^\downarrow > 0.5$, the double occupation density at the reservoir does not vanish and is transported into the system. Hence the system can exhibit total densities larger than one if its bulk behavior is determined by the left boundary. In this case, the description we introduce below for the regime of intermediate coupling applies.

IV. CURRENT-DENSITY RELATION

The interaction between neighboring particles directly affects the transport properties of the system. The current's dependence on the bulk densities is very sensitive on the coupling. Above a certain value the current-density relation changes qualitatively resulting in a rich phase behavior as we show in the following section.

A. One-site cluster approximation

With increasing coupling strength U, the occupation numbers of the same site on different lanes become more and more correlated and a simple mean-field approximation fails. However, by employing a one-site cluster approximation we obtain a valuable expression for the currents depending on the bulk densities as demonstrated in [7]. To account for correlations between the same site on different lanes, we introduce, besides the single particle densities $\rho_i^\uparrow = \langle n_i^\uparrow \rangle, \rho_i^\downarrow = \langle n_i^\downarrow \rangle$, the double occupation density on site i, $\kappa_i := \langle n_i^\uparrow n_i^\downarrow \rangle$ as an additional variable [43].

Then, the probabilities for the other three particle configurations on site i, unoccupied or occupied by one particle either on the upper or the lower lane, can be expressed in terms of $\rho_i^\uparrow, \rho_i^\downarrow$, and κ_i. We neglect all other correlations and employ the standard decoupling approximation scheme there.

Assuming spatially homogeneous density profiles, the currents on the upper and the lower lane can be expressed in terms of $\rho^\uparrow, \rho^\downarrow$, and κ. The details of the calculations are presented in the Appendix. We obtain

$$\begin{aligned} j^\uparrow &= \rho^\uparrow(1 - \rho^\uparrow) + \mu, \\ j^\downarrow &= \rho^\downarrow(1 - \rho^\downarrow) + \mu, \end{aligned} \tag{6}$$

where $\rho^{\uparrow(\downarrow)}(1 - \rho^{\uparrow(\downarrow)})$ is the particle current known from TASEP and $\mu = \kappa - \rho^\uparrow \rho^\downarrow$ is the correlation correction reducing the current compared to the case without any coupling. Here, the double occupation density κ is the positive solution of the quadratic equation,

$$0 = (1 - e^{-U})\kappa^2 + [1 - (1 - e^{-U})\rho]\kappa - e^{-U}\rho^\uparrow \rho^\downarrow, \tag{7}$$

where $\rho = \rho^\uparrow + \rho^\downarrow$ is the total density. We will employ these results in the following section within the framework of an extremal-current principle to investigate the phase behavior as a function of the coupling strength.

In agreement with the considerations in the previous section, the double occupation density vanishes in the limit $U \to \infty$, while it simplifies to $\kappa = \rho^\uparrow \rho^\downarrow$ for $U \to 0$. The latter limit connects the one-site cluster approximation to the simple mean-field approximation, which is accurate for small potentials.

B. Dependence of the currents on the potential U

The current displays a sensitive dependence on the strength of interaction, U. For small interaction strength, the currents on each lane are almost independent of the density on the other lane. Indeed, these currents are approximately parabolic with respect to the density in the respective lane; see Fig. 4(a). The maximal current on the upper channel $j_{max}^\uparrow$ occurs for $\rho^\uparrow = 1/2, \rho^\downarrow = 0$, and $\rho^\uparrow = 1/2, \rho^\downarrow = 1$ since the obstruction does not affect the transport on the upper lane for these densities. With an increase in the potential U, the particle flux decreases, in particular, for densities around $\rho^\uparrow = \rho^\downarrow = 1/2$, as shown in Fig. 4(b).

This behavior is also reflected in the total current as shown in Figs. 4(c) and 4(d). For small potentials, the total current

(a) Single-channel current, $j^\uparrow$, for $U = 0.3$

(b) Single-channel current, $j^\uparrow$, for $U = 2$

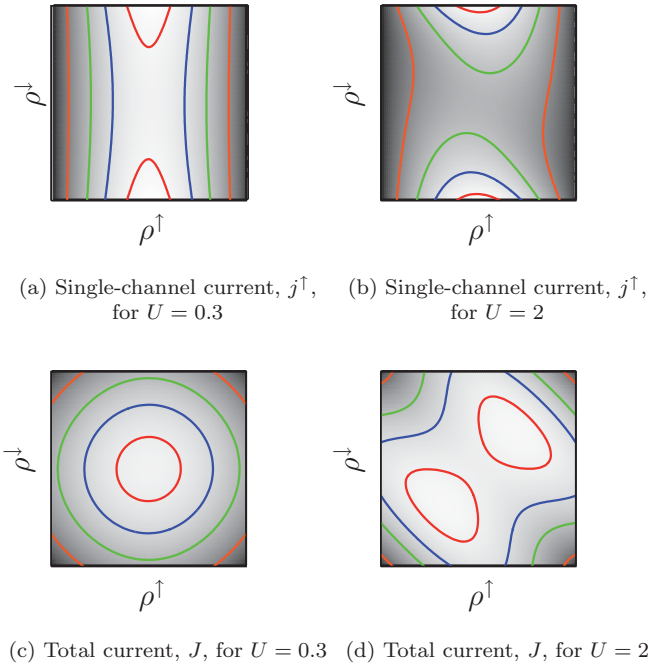(c) Total current, J, for $U = 0.3$ (d) Total current, J, for $U = 2$

FIG. 4. (Color online) Contour plots for the individual (top) and the total current (bottom), depending on the bulk densities, for $U = 0.3$ (left) and $U = 2$ (right) using Eq. (6). In gray scale, black corresponds to vanishing current, and white to the respective maximal currents $j_{max}^\uparrow, J_{max}$. The colored (gray) contour lines indicate currents of value $0.95 \cdot j_{max}^\uparrow$ and $0.95 \cdot J_{max}$ (red), $0.8 \cdot j_{max}^\uparrow$ and $0.8 \cdot J_{max}$ (blue), $0.5 \cdot j_{max}^\uparrow$, and $0.5 \cdot J_{max}$ (green), $0.3 \cdot j_{max}^\uparrow$ and $0.3 \cdot J_{max}$ (orange) from inside to outside. Increasing the obstruction strength, the single maximum splits into two, separated by a saddle. The transition happens at a critical value of the interaction, $U_C = \ln 4 \approx 1.4$.

in bulk displays a single maximum located at $\rho^\uparrow = \rho^\downarrow = 1/2$; see Fig. 4(c). In this regime the potential only affects the value of the maximum but not its position, i.e., it does not change the topology of the phase diagrams. Beyond a critical value of the potential, $U_C = \ln 4 \approx 1.4$, the total current displays a qualitatively different behavior, as has been described in Ref. [7]. At the critical value, two maxima separated by a saddle evolve in the current-density relation for the total current; see Fig. 4(d). The location of these maxima is evaluated in the Appendix. Upon further increasing U, the maxima move apart. In the limit of large potentials two elongated maxima evolve and the saddle becomes a valley located at $\rho^\uparrow = 1 - \rho^\downarrow$. The bimodal structure leads to a richer phase diagram than in the weak coupling regime, $U < \ln 4$. Similar extrema in the currents were found previously for one-channel systems, e.g., when next-nearest-neighbor interactions are taken into account [44].

C. Influence of the potential U on the right boundary

At the right boundary ($i = L$) exiting rates control the currents out of the system:

$$j_{EX}^\uparrow = \beta^\uparrow \rho_L^\uparrow,$$
$$j_{EX}^\downarrow = \beta^\downarrow \rho_L^\downarrow. \tag{8}$$

These currents are either determining the system or are virtual currents which are important for predicting the phase behavior in the system as explained in the following section. If these exiting currents also set the bulk currents, i.e., if $j^\uparrow = j_{EX}^\uparrow$ and $j^\downarrow = j_{EX}^\downarrow$, we can compute the bulk densities (which then equal the densities at the right boundary) depending on the exiting rates via Eq. (8). The densities at the right boundary also play a key role for determining the phase diagrams, as we will see below. For a small coupling strength, we find $\rho^{\uparrow(\downarrow)} \approx 1 - \beta^{\uparrow\downarrow}$, as familiar from TASEP. The transport properties change rapidly when repulsion between particles increases. In particular, for potentials larger than U_C the double-maxima structure of the bulk current comes into play and causes a discontinuous dependence of the bulk density on the exiting rates. Such a jump in the densities is exemplified in Fig. 5 for the case of equal exiting rates.
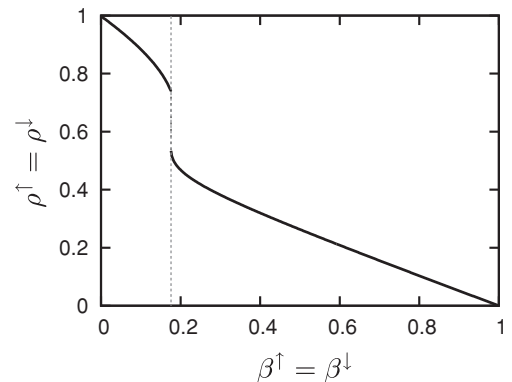

FIG. 5. The dependence of the bulk densities, $\rho^\uparrow = \rho^\downarrow$, on equal exiting rates $\beta^\uparrow = \beta^\downarrow$ for systems determined by the right boundary. It is obtained by evaluating Eq. (8). The interaction strength $U = 3.0$ is above the critical value U_C.

V. PHASE BEHAVIOR

The system's phases depend on the boundary conditions as well as on the strength of internal obstruction. In the following, we employ the extremal-current principle to evaluate the analytic expressions for the currents obtained in the previous section to get insight into the phase behavior. We then discuss these phases and point out some special features arising from the coupling.

A. Extremal-current principle

The extremal-current principle (ECP) often governs the phase behavior of driven diffusive systems [13,44,45]. So far the ECP has only been established for one-dimensional systems. Here we describe a two-dimensional generalization and show that it successfully describes the phase behavior of our two-lane model. We start with a short description of the standard one-dimensional ECP, and then extend it to two coupled lanes.

The ECP for transport on a single lane can be formulated by considering two characteristic velocities. The first is the collective velocity, $v_c = \partial j / \partial \rho$, which reveals information of the stability of a given bulk density ρ against perturbations: only densities with $v_c = 0$ (as well as those determined by the boundaries) are stable. The second quantity is the shock velocity $v_s = [j(\rho_1) - j(\rho_2)]/(\rho_1 - \rho_2)$ that gives the direction in which a domain wall between two densities, ρ_1 and ρ_2, travels. In this way, v_s determines which of both densities, ρ_1 or ρ_2, dominates. To find the system's bulk density, it therefore suffices to first identify the stable densities, using the collective velocity, and then, by pairwise comparison via the shock velocity, single out the bulk density. These considerations are summarized by the extremal-current principle:

$$
\begin{aligned}
j &= \max_{\rho \in [\rho_+, \rho_-]} j(\rho) \quad \text{for} \quad \rho_+ > \rho_-, \\
j &= \min_{\rho \in [\rho_+, \rho_-]} j(\rho) \quad \text{for} \quad \rho_+ < \rho_-,
\end{aligned}
\tag{9}
$$

where ρ_+ is the density at the left boundary, and ρ_- is the density at the right boundary. Hence the system is either determined by the entering or exiting current or by an extremal current corresponding to a density in between the boundary densities.

On two coupled lanes, the currents in bulk are generically influenced by both lanes. We therefore have to consider the dependence of the currents on both $\rho^\uparrow$ and $\rho^\downarrow$. As in the one-dimensional case, either the maximal or the minimal (total) current (see Fig. 6, blue and green area) determines the transport in the system, and the velocities v_c and v_s govern which of both scenarios is realized. However, in order to decide which of both cases applies it is no longer sufficient to compare the densities at the boundaries. Because of many potentially conflicting cases a rigorous derivation of the ECP provides a considerable challenge. We have, however, observed that the following intuitive version of the ECP describes our model's phase behavior in the full parameter space.

In the one-dimensional ECP an extremal current belonging to a density in the interval determines the system. In the two-dimensional scenario the interval is replaced by a rectangle
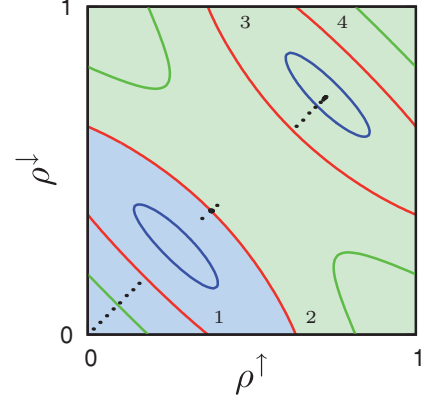

FIG. 6. (Color online) Contour plot of the total current, depending on the bulk densities. The bulk densities emerging for special values of equal reservoir densities ($\rho_{\text{res}}^\uparrow = \rho_{\text{res}}^\downarrow$), namely continuously increasing from 0 to 1, are displayed as black dots. The other parameters are $\beta^\uparrow = \beta^\downarrow = 0.3$ and $U = 3.0$. The red contour line corresponds to the total exiting current as emerges if the right boundary determines the bulk densities. It marks the transition from the minimal (blue area, lower left corner) to the maximal (green area, upper right corner) current principle and two phase transitions. In the lower left corner the system is in the IN/IN phase, crossing the red contour line it enters the EX/EX phase. Upon further increase in the reservoir densities the IN/IN phase is reached again in the upper right corner, before the MC/MC phase arises where the densities are limited by the bulk properties.

bounded by the boundary densities, $(\rho_L^\uparrow, \rho_L^\downarrow)$ and $(\rho_{\text{res}}^\uparrow, \rho_{\text{res}}^\downarrow)$. Depending on the boundary conditions either the minimal or the maximal current gives the bulk currents. The currents, which have to be considered are the entering and the exiting current or a mixture of both, i.e., one lane is determined by the left while the other one is determined by the right boundary. The exiting current can be calculated by equating Eqs. (6) and (8) with Eq. (7). For the specific example $U = 3, \beta^\uparrow = \beta^\downarrow = 0.3$, the corresponding contour line of the current-density relation consists of several disjoint lines; see Fig. 6 where the red line has four parts which are denoted as 1, 2, 3, and 4. Then, the part that includes the point $(\rho_L^\uparrow, \rho_L^\downarrow)$ marks the boundary where the maximal or minimal current is selected. In the example discussed here this boundary is given by line 2 in Fig. 6. The extrema to be considered for the ECP are located at the boundary of the rectangle given by $(\rho_L^\uparrow, \rho_L^\downarrow)$ $(\rho_{\text{res}}^\uparrow, \rho_{\text{res}}^\downarrow)$, or at the extremum on the rectangle. This extremum can be inside the rectangle or also at its boundary.

To illustrate the extremal-current principle we consider a path where the reservoir densities are gradually increased along the diagonal $\rho_{\text{res}} = \rho_{\text{res}}^\uparrow = \rho_{\text{res}}^\downarrow$ for fixed exiting rates and interaction strength. Even though we choose this path as an example, our results hold for arbitrary boundary conditions as exemplified in the following. Figure 7 displays the bulk densities and the phase transitions that occur. For small reservoir densities the minimal current is selected, which is given by the left reservoirs there. Upon crossing the current contour line (1) for the first time, the left reservoir current is larger than the exiting current, and transport is determined by the exiting rates. Crossing the contour line that includes
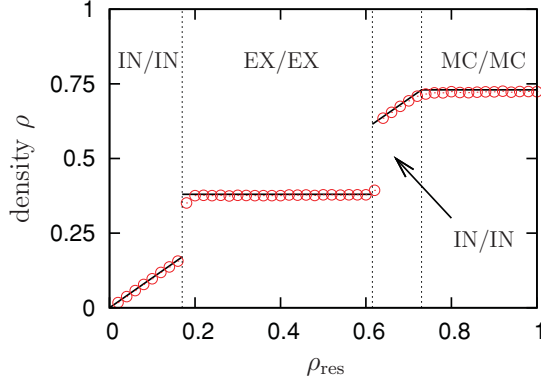
FIG. 7. (Color online) Average bulk densities for increasing reservoir densities $\rho_{res} = \rho_{res}^{\uparrow} = \rho_{res}^{\downarrow}$. The parameters are set to $\beta^{\uparrow} = \beta^{\downarrow} = 0.3$ and $U = 3$; the situation corresponds to Fig. 6. The phases introduced here are discussed in Sec. V B. Red (gray) circles denote simulation results; black lines correspond to analytical predictions from the ECP.

the point $(\rho_L^{\uparrow}, \rho_L^{\downarrow})$ (line 2), does not give rise to a phase transition, since now the maximum current determines the bulk current. In this domain the exiting current is larger than the left reservoir current. The next phase transition happens when the current at the left boundary exceeds the exiting current. Again, the phase transition occurs at a segment of the red contour line (line 3). Upon a further increase, the second maximum of the current-density relation is reached, and the maximal-current phase is entered. For reservoir densities larger than $(\rho_I^{\uparrow}, \rho_I^{\downarrow})$, i.e., for the maximum bulk current, see Eq. (A6) in the Appendix, a maximum current is attained.

B. Phases

As discussed above the system either adopts its minimal or maximal current, depending on the boundary conditions. These extremal currents can be either given by one boundary or by an extremum of the current-density relation itself. Hence we can distinguish two classes of phases in the system, boundary- and bulk-induced phases. The first one is highly sensitive to small changes in the boundary conditions, while in the latter one the densities are determined by the bulk properties and do not depend on the entering and exiting parameters.

1. Boundary-induced phases

The boundary-induced phases depend either on the entering or exiting processes, and we consequently differentiate between IN and EX phases. In our model, we employ particle reservoirs at the left boundary, but exiting rates at the right one. As a consequence the left and the right boundary influence the bulk densities in qualitatively different ways. Indeed, in the case where both lanes are determined be the left boundary (IN/IN phase), the bulk densities are given by the reservoirs densities, $\rho^{\uparrow} = \rho_{res}^{\uparrow}, \rho^{\downarrow} = \rho_{res}^{\downarrow}$. In contrast, if a system is in the EX/EX phase, only the total current is fixed to the value given by the right boundary, whereas the bulk densities also depend on the reservoir densities at the left boundary, for $\rho_{res}^{\uparrow} \lessgtr \rho_{res}^{\downarrow}$ holds $\rho^{\uparrow} \lessgtr \rho^{\downarrow}$. Further mixed phases (IN/EX or EX/IN) may
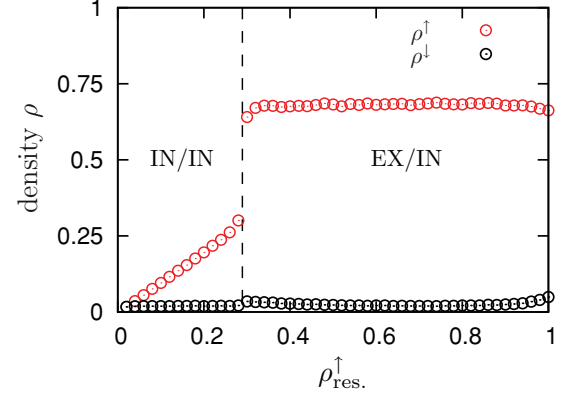

FIG. 8. (Color online) Average bulk densities for different upper reservoir densities $\rho_{res}^{\uparrow}$. Parameters are $\rho_{res}^{\downarrow} = 0.02$, $\beta^{\uparrow} = \beta^{\downarrow} = 0.3$, $U = 3.0$. If both reservoir densities are small, the system is in the IN/IN phase where both bulk densities are given by the reservoirs. This changes for larger $\rho_{res}^{\uparrow}$. While the lower lane is still determined by the left boundary, the upper lane is governed by the right boundary (EX/IN phase).

become relevant where the current on one lane is determined by the left boundary and the current on the other is fixed by the exiting current.

The IN/IN and the EX/IN phase are exemplified in Fig. 8 where we show the average bulk densities depending on the upper reservoir density $\rho_{res}^{\uparrow}$. Parameters are chosen such that a transition from the IN/IN to the EX/IN phase emerges at a certain value of $\rho_{res}^{\uparrow}$. Only in the IN/IN phase do the bulk densities vary when changing the upper reservoir density $\rho_{res}^{\uparrow}$; in the EX/IN phase they are almost undisturbed by changes in $\rho_{res}^{\uparrow}$.

2. Bulk-induced phases

In the bulk-determined phases, the current is given by an extremum of the current-density relation. Here we restrict the discussion to the case where a maximum occurs (MC phase), yet one can find parameter regions where a saddle fixes the phase behavior [40].

In the maximum-current phase a localized domain wall can emerge, separating a high-density regime at the left and a low-density regime at the right; see Fig. 9. This scenario, previously found in Ref. [13], occurs if both maxima $(\rho_I^{\uparrow}, \rho_I^{\downarrow})$ and $(\rho_{II}^{\uparrow}, \rho_{II}^{\downarrow})$, Eq. (A6) in the Appendix, are accessible. Each domain along the lane then corresponds to one of the maximal currents. In particular, the current is continuous at the domain wall. In Fig. 9, the reservoir density at the left boundary is larger than the density corresponding to the second maximum, while the density at the right boundary is smaller than the density corresponding to the first maximum. Hence in the vicinity of each boundary the density which is closer to the respective boundary density arises. Depending on the exact values of the boundary densities, the domain wall is located between the left hand side and the middle of the system. Increasing the reservoir densities the domain wall moves further to the right. In Fig. 7, the MC/MC phase is shown for symmetric boundary conditions. The black line denotes the analytically obtained density corresponding to the second maximum of the
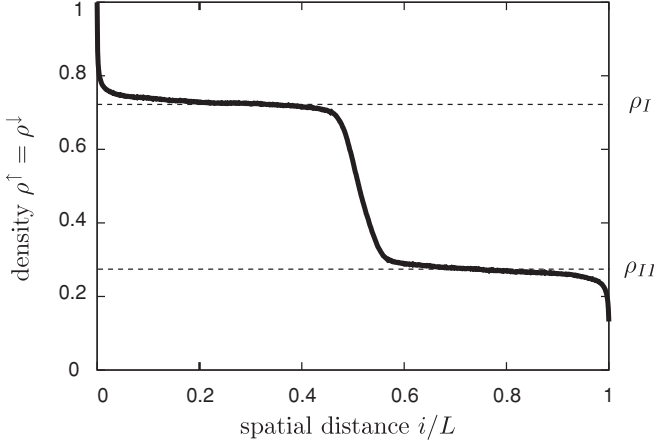
FIG. 9. Density profile of a state exhibiting maximal current. The parameters are $\rho_{\text{res}}^{\uparrow} = \rho_{\text{res}}^{\downarrow} = 1$, $\beta^{\uparrow} = \beta^{\downarrow} = 1$, $U = 3.0$, and $L = 1000$. The current remains spatially constant while the density shows a high value at the left and a low value at the right. Both densities correspond to maxima in the current-density relation, ρ_I, ρ_{II}. An unusual localized domain wall forms between them; see text.
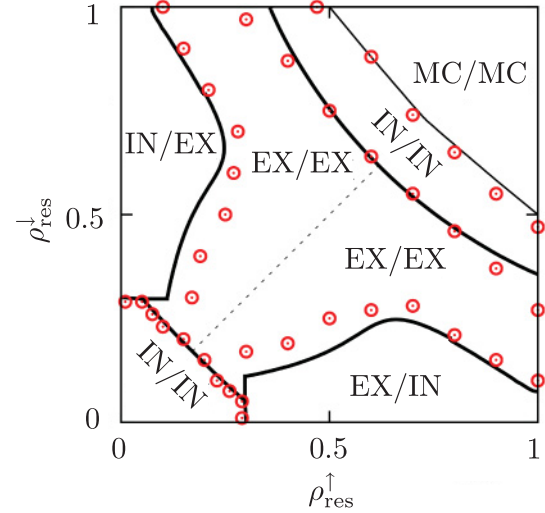

FIG. 10. (Color online) A generic phase diagram with the reservoir densities as control parameters. The exiting rates are fixed to $\beta^{\uparrow} = \beta^{\downarrow} = 0.3$ and the interaction strength is set to $U = 3.0$. The red (gray) dots denote simulation results of the transition lines, while the black lines are calculated employing the ECP. Besides the combinations of phases which are determined by entering or exiting currents, phases which do not exist for $U < \ln 4$ are also present. Namely, a second IN/IN phase, which exhibits a high density, and the MC/MC, where the maximal current determines the bulk densities, occur.

current density relation. It is in excellent agreement with the simulation results.

C. Phase diagrams

Employing the extremal-current principle, the phase diagrams can be characterized completely also for unequal boundary densities.. As described above, there exist several phases which are either determined by the boundaries or by the bulk transport properties of the system. According to the ECP the phase transition lines are given by equating the entering and exiting currents or by the structure of the current-density relation. The bulk current dominates if the maximum on the rectangle bounded by the corners $(\rho_{\text{res}}^{\uparrow}, \rho_{\text{res}}^{\downarrow})$, $(\rho_L^{\uparrow}, \rho_L^{\downarrow})$ is not given by either of these points. It is clear that a transition from a left-reservoir or right-exiting-currents dominated phase to a maximum-current phase can emerge only if the extremum traverses the boundary of the rectangle considered. Further transitions to an IN/EX and EX/IN phase are identified using again the extremal-current principle employing contour lines corresponding to the total current in the mixed phases.

In Fig. 10 we exemplify a phase diagram depending on unequal reservoir densities. The exiting rates are fixed to $\beta^{\uparrow} = \beta^{\downarrow} = 0.3$ and the potential is set to $U = 3$, a value where the current-density relation shows two maxima. The parameters are identical to the ones of Figs. 6 and 7. In Fig. 10, the stochastic simulations (red dots) are in good agreement with the analytic calculations (black lines). Because the latter ones were obtained employing the ECP also for unequal reservoir densities, the strength and generality of the ECP can be confirmed. Due to the symmetry between both lanes, the phase diagram is symmetric along its diagonal, $\rho_{\text{res}}^{\uparrow} = \rho_{\text{res}}^{\downarrow}$.

In the lower left corner, where both reservoir densities are small, both channels are determined by the entering current (IN/IN phase). Increasing only one reservoir density, the minimal current is no longer given by the entering current on the respective lane. Hence the system reaches the EX/IN

phase (IN/EX phase). The phase-transition lines between the IN/IN and IN/EX phase, as well as the ones between the IN/EX and the EX/EX phase, are given by contour lines of the current on an individual lane, Eq. (6). In the middle of the phase diagram, both channels are determined by the exiting currents. As mentioned above, only the total current is fixed in this phase, in contrast to the bulk densities which also depend on the reservoir densities at the left boundary. The dotted line marks the region where the bulk densities on both channels are equal. On this line the bulk densities can be calculated employing Eq. (8). For a further increase in the reservoir densities, the IN/IN phase arises again where the bulk currents as well as the bulk densities are given by the left boundary. This phase would not arise if we had chosen entering rates, rather than particle reservoirs, at the left boundary, because boundary densities larger than 1/2 would then not emerge. In our case, such large densities cause currents larger than the entering current. These dominate the system according to the extremal-current principle. For even larger reservoir densities the crest of the current-density relation, which marks the phase transition from the IN/IN to the MC/MC phase, is reached, and the bulk densities remain constant at the values where the second maximum is located.

VI. SUMMARY AND CONCLUSION

In this paper we have examined a driven two-channel model where the motion of particles along both channels is coupled via a repulsive short-range interaction. The latter causes intriguing phenomena and phases. Varying the strength of particle obstruction, three regimes of qualitatively different

behavior evolve. First, for small coupling the system approximately acts as two uncoupled lanes, i.e., the phases and phase diagram qualitatively correspond to the ones already known from TASEP. These results can be confirmed by employing a simple mean-field approach or a one-site cluster approximation. Second, for moderate interaction strength the transport properties of the system are strongly influenced by the obstruction between neighboring particles. This regime emerges around a critical interaction strength, $U_C = \ln 4$ [7], where a single maximum of the current-density relation splits into two, separated by a saddle. Third, when the obstruction is large, the two coupled lanes effectively behave as a single one. In this case, we have identified a mapping from the parameters governing entering and exiting processes in our system to effective rates for a single-lane TASEP. This mapping then allows us to carry over known results from TASEP, such as its phase diagram. Hence for different strengths of the obstruction a variety of peculiar phases surface which can be accessed by manipulating the system at the boundary only. The boundary-sensitive phases respond gradually upon tuning the left reservoir or the exiting rates, whereas the maximal-current phase is robust against such changes.

In contrast to previous work [7], we explicitly investigated the two-channel system with a broken lane symmetry. We thereby followed the proposition in [7] that the ECP might be generic for multichannel system. As a key result we indeed derive a suitable generalization of the ECP to two dimensions. We thereby approve that not the densities but the currents govern the transitions between the minimal and the maximal current principle, a distinction that cannot be made within one-dimensional or symmetric situations. The accuracy with which the system's phase behavior can be predicted with our two-dimensional ECP is astonishing and suggests it for further applications. In further contrast to [7] we specifically investigated the dependence on the potential U. For small potentials the system's behavior is not sensitive on whether reservoir or rates are chosen at the boundaries. However, for intermediate and large potentials, reservoirs or rates at the boundaries make a difference. For example, the system does not behave like a one-channel system for large potentials if reservoirs are chosen instead of rates at the right boundary, as has been done in [7]. Because we employ exiting rates at the right boundary, we observe interesting effects such as a strong impact of the potential U on the exiting current (Fig. 5), and two transitions instead of one in the bulk densities upon increasing U (Fig 3).

It would be interesting to consider also lane changes (respectively, spin flips) of the particles as they proceed along the channel. Such events are expected in realistic applications such as intracellular transport, highway traffic on multiple lanes, or hopping transport of electrons through a chain of quantum dots. The correlations induced by frequent lane changes [32,46], ignoring mutual obstruction, are accurately described by a one-site cluster approximation similar to the one we employed. Yet, for rare lane changes a simple mean-field approximation suffices to describe the arising localized domain walls [12]. The combination of obstruction, lane switching, and possibly also defects constitutes a promising route to discover novel and unexpected collective phenomena in driven transport.

In conclusion, we have shown that the ECP can be generalized to higher dimensions to serve as an appropriate tool for the investigation of driven multichannel systems. We therefore think that extremal-current principle is a promising starting point to achieve a deeper understanding of complex transport phenomena.

APPENDIX: CURRENT-DENSITY RELATION

In this Appendix, we derive an analytic description for the current-density relation within a one-site cluster approximation. The individual currents onto a site i can be obtained be evaluating the particle fluxes onto this site,

$$
\begin{aligned}
j_i^\uparrow &= \langle e^{-U}(n_{i-1}^\uparrow - n_{i-1}^\uparrow n_{i-1}^\downarrow)(n_i^\uparrow - n_i^\uparrow n_i^\downarrow)\rangle \\
&+ \langle (n_{i-1}^\uparrow - n_{i-1}^\uparrow n_{i-1}^\downarrow)(1 - n_i^\uparrow - n_i^\downarrow + n_i^\uparrow n_i^\downarrow)\rangle \\
&+ \langle n_{i-1}^\uparrow n_{i-1}^\downarrow (1 - n_i^\uparrow)\rangle,
\end{aligned} \tag{A1}
$$

and similarly for $j_i^\downarrow$. This expression is evaluated employing the one-site cluster approximation discussed in Sec. IV A. The essence of the approach consists of considering all four possible states of the two opposing sites, whereas all correlations between neighboring sites are factorized. Thus a complete description is achieved in terms the mean double-occupation density $\kappa_i = \langle n_i^\uparrow n_i^\downarrow \rangle$ besides the average densities $\rho_i^\uparrow = \langle n_i^\uparrow \rangle$ and $\rho^\downarrow = \langle n_i^\downarrow \rangle$. Then the closure relation for the currents is derived,

$$
\begin{aligned}
j_i^\uparrow &= e^{-U}(\rho_{i-1}^\uparrow - \kappa_{i-1})(\rho_i^\uparrow - \kappa_i) \\
&+ (\rho_{i-1}^\uparrow - \kappa_{i-1})(1 - \rho_i^\uparrow - \rho_i^\downarrow + \kappa_i) \\
&+ \kappa_{i-1}(1 - \rho_i^\uparrow).
\end{aligned} \tag{A2}
$$

Similar to Eq. (A1), the time evolution for the double-occupation density κ_i involves averages of products of occupation variables n_i. Within the same truncation of the hierarchy, one finds

$$
\begin{aligned}
\partial_t \kappa_i &= e^{-U}(\rho_{i-1}^\uparrow - \kappa_{i-1})(\rho_i^\downarrow - \kappa_i) \\
&+ e^{-U}(\rho_{i-1}^\downarrow - \kappa_{i-1})(\rho_i^\uparrow - \kappa_i) \\
&+ \kappa_{i-1}(\rho_i^\uparrow + \rho_i^\downarrow - 2\kappa_i) \\
&- \kappa_i(2 - \rho_{i+1}^\uparrow - \rho_{i+1}^\downarrow).
\end{aligned} \tag{A3}
$$

In the steady state and for spatially homogeneous density profiles, the double occupation density κ obeys a quadratic equation with solution

$$
\kappa = \frac{\lambda\rho - 1 + \sqrt{(\lambda\rho - 1)^2 + 4\lambda(1-\lambda)\rho^\uparrow \rho^\downarrow}}{2\lambda}. \tag{A4}
$$

Here, $\lambda = 1 - e^{-U}$ corresponds to the inverse dwell time in the obstructed case and $\rho = \rho^\uparrow + \rho^\downarrow$ to the total density. Combining this result with the closure relation for the current,

Eq. (A2), the closed expression for the current-density relation follows,

$$j^\uparrow = \rho^\uparrow(1 - \rho^\uparrow - \rho^\downarrow) + \kappa,$$
$$j^\downarrow = \rho^\downarrow(1 - \rho^\uparrow - \rho^\downarrow) + \kappa. \quad (A5)$$

The total current $J = j^\uparrow + j^\downarrow$ displays a single maximum for small interactions U located at $\rho^\uparrow = \rho^\downarrow = 1/2$. This

maximum is replaced a saddle for strong coupling and two maxima of equal height appear on the diagonal. These new maxima are located at

$$\rho^\uparrow_{I,II} = \rho^\downarrow_{I,II} = \frac{1}{2} \pm \frac{\sqrt{1 - 5e^{-U} + 4e^{-2U}}}{4(1 - e^{-U})}. \quad (A6)$$

These solutions are only real for potentials larger than the critical value, $U_C = \ln 4$.

[1] B. Schmittmann and R. Zia, in *Phase Transitions and Critical Phenomena*, edited by C. Domb and J. Lebowitz (Academic Press, London, 1995), Vol. 17, pp. 1–120.
[2] G. Schütz, in *Phase Transitions and Critical Phenomena* (Ref. [1]), Vol. 19, pp. 1–251.
[3] N. Hirokawa, Science **279**, 519 (1998).
[4] T. Chou and D. Lohse, Phys. Rev. Lett. **82**, 3552 (1999).
[5] J. Howard, *Mechanics of Motor Proteins and the Cytoskeleton* (Sinauer, Sunderland, MA, 2001).
[6] H. Hinsch, R. Kouyos, and E. Frey, in *Traffic and Granular Flow '05*, edited by A. Schadschneider, T. Pöschel, R. Kühne, M. Schreckenberg, and D. E. Wolf (Springer, New York, 2006), pp. 205–202.
[7] V. Popkov and I. Peschel, Phys. Rev. E **64**, 026126 (2001).
[8] D. Helbing, Rev. Mod. Phys. **73**, 1067 (2001).
[9] D. Chowdhury, L. Santen, and A. Schadschneider, Phys. Rep. **329**, 199 (2000).
[10] B. Schmittmann, J. Krometics, and R. K. P. Zia, Europhys. Lett. **70**, 299 (2005).
[11] S. Katz, J. L. Lebowitz, and H. Spohn, Phys. Rev. B **28**, 1655 (1983).
[12] T. Reichenbach, T. Franosch, and E. Frey, Phys. Rev. Lett. **97**, 050603 (2006).
[13] J. Krug, Phys. Rev. Lett. **67**, 1882 (1991).
[14] C. MacDonald, J. Gibbs, and A. Pipkin, Biopolymers **6**, 1 (1968).
[15] B. Derrida and J. L. Lebowitz, Phys. Rev. Lett. **80**, 209 (1998).
[16] B. Derrida, M. Evans, V. Hakim, and V. Paquier, J. Phys. A **26**, 1493 (1993).
[17] A. Vilfan, E. Frey, F. Schwabl, M. Thormählen, Y. Song, and E. Mandelkow, J. Mol. Biol. **312**, 1011 (2001).
[18] A. Parmeggiani, T. Franosch, and E. Frey, Phys. Rev. Lett. **90**, 086601 (2003).
[19] S. Klumpp and R. Lipowsky, J. Stat. Phys. **113**, 233 (2003).
[20] K. Nishinari, Y. Okada, A. Schadschneider, and D. Chowdhury, Phys. Rev. Lett. **95**, 118101 (2005).
[21] P. Greulich, A. Garai, K. Nishinari, A. Schadschneider, and D. Chowdhury, Phys. Rev. E **75**, 041905 (2007).
[22] A. Parmeggiani, T. Franosch, and E. Frey, Phys. Rev. E **70**, 046101 (2004).

[23] P. Pierobon, E. Frey, and T. Franosch, Phys. Rev. E **74**, 031920 (2006).
[24] G. Tripathy and M. Barma, Phys. Rev. Lett. **78**, 3039 (1997).
[25] P. Pierobon, M. Mobilia, R. Kouyos, and E. Frey, Phys. Rev. E **74**, 031906 (2006).
[26] P. Greulich and A. Schadschneider, J. Stat. Mech. (2008) P04009.
[27] C. Kural, H. Kim, S. Syed, G. Goshima, V. I. Gelfand, and P. R. Selvin, Science **308**, 1469 (2005).
[28] M. J. I. Müller, S. Klumpp, and R. Lipowsky, Proc. Natl. Acad. Sci. USA **105**, 4609 (2008).
[29] W. Knospe, L. Santen, A. Schadschneider, and M. Schreckenberg, J. Phys. A **35**, 3369 (2002).
[30] T. Reichenbach, E. Frey, and T. Franosch, New J. Phys. **9**, 159 (2007).
[31] T. Reichenbach, T. Franosch, and E. Frey, Eur. Phys. J. E **27**, 47 (2008).
[32] E. Pronina and A. B. Kolomeisky, J. Phys. A **37**, 9907 (2004).
[33] R. Jiang, M.-B. Hu, Y.-H. Wu, and Q.-S. Wu, Phys. Rev. E **77**, 041128 (2008).
[34] T. Mitsudo and H. Hayakawa, J. Phys. A **38**, 3087 (2005).
[35] R. Juhasz, Phys. Rev. E **76**, 021117 (2007).
[36] D. Chowdhury, A. Garai, and J.-S. Wang, Phys. Rev. E **77**, 050902 (2008).
[37] K. Tsekouras and A. B. Kolomeisky, J. Phys. A **41**, 465001 (2008).
[38] E. Pronina and A. B. Kolomeisky, J. Phys. A **40**, 2275 (2007).
[39] R. Hanson, L. Kouwenhoven, J. Petta, S. Tarucha, and L. Vandersypen, Rev. Mod. Phys. **79**, 1217 (2007).
[40] A. Melbinger, Diploma thesis, Ludwig-Maximilians-Universität München, 2007.
[41] D. T. Gillespie, J. Comput. Phys. **22**, 403 (1976).
[42] D. T. Gillespie, J. Phys. Chem. **81**, 2340 (1977).
[43] D. ben-Avraham and J. Köhler, Phys. Rev. A **45**, 8358 (1992).
[44] V. Popkov and G. M. Schütz, Europhys. Lett. **48**, 257 (1999).
[45] J. S. Hager, J. Krug, V. Popkov, and G. M. Schütz, Phys. Rev. E **63**, 056110 (2001).
[46] E. Pronina and A. B. Kolomeisky, Physica A **372**, 12 (2006).